ELSEVIER

Earth and Planetary Science Letters 209 (2003) 351–360

EPSL

www.elsevier.com/locate/epsl

Deformation of $(Mg_{0.9},Fe_{0.1})SiO_3$ Perovskite aggregates up to 32 GPa

Sébastien Merkel [a,b,*], Hans Rudolf Wenk [c], James Badro [d], Gilles Montagnac [b], Philippe Gillet [b], Ho-kwang Mao [a], Russell J. Hemley [a]

[a] *Geophysical Laboratory, Carnegie Institution of Washington, Washington, DC, USA*
[b] *Laboratoire des Sciences de la Terre, UMR 5570 CNRS, École normale supérieure de Lyon, Lyon, France*
[c] *Department of Earth and Planetary Science, University of California, Berkeley, CA, USA*
[d] *Laboratoire de Minéralogie-Cristallographie, Université Paris VI, Paris, France*

Received 18 September 2002; received in revised form 3 February 2003; accepted 11 February 2003

Abstract

Room temperature investigations on the shear stress and deformation mechanisms of $(Mg_{0.9}Fe_{0.1})SiO_3$ perovskite are performed in situ up to 32 GPa using radial X-ray diffraction and the diamond anvil cell as a deformation apparatus. The uniaxial stress supported by the perovskite aggregate is found to increase continuously with pressure up to 10.9($\pm$1.9) GPa at 32($\pm$1) GPa. Our measurements show no development of significant lattice preferred orientations in the sample, which indicates that deformation by dislocation glide is not the dominant deformation mechanism under these conditions. Assuming that the underlying cause for seismic anisotropy in the deep Earth is elastic anisotropy combined with lattice preferred orientation, our results indicate that silicate perovskite deformed under the conditions of this experiment would not be the source of seismic anisotropy.
© 2003 Elsevier Science B.V. All rights reserved.

Keywords: high pressure; deformation; perovskite; shear strength; texture; anisotropy

1. Introduction

Silicate perovskite is the most abundant mineral in the Earth's lower mantle and, although it has been subjected to numerous experimental and theoretical investigations, its rheological properties remain poorly understood. Information on the shear strength and deformation mechanisms of $(Mg,Fe)SiO_3$ is crucial for constraining mantle convection and the development of seismic anisotropy in the deep Earth (e.g. [1]). However, $(Mg,Fe)SiO_3$ perovskite is known to be extremely difficult to study with conventional laboratory deformation experiments: for the most part, only analogs with the perovskite structure have been investigated under the assumption that such materials have similar mechanical properties. From such analog studies, creep laws and deformation mechanisms of silicate perovskite were implied (see [2–10] and references therein). Despite consid-

* Corresponding author. Present address: Institute for Solid State Physics, University of Tokyo, Kashiwa, Chiba 277-8581, Japan. Tel.: +41-4-7136-3231; Fax: +41-4-7136-3230.
E-mail address: smerkel@issp.u-tokyo.ac.jp (S. Merkel).

0012-821X/03/$ – see front matter © 2003 Elsevier Science B.V. All rights reserved.
doi:10.1016/S0012-821X(03)00098-0

erable efforts, these experiments have demonstrated that the analog approach is problematic [4]. Silicate perovskite is very unstable at ambient pressure and it is very difficult to obtain high quality and large dimension samples. Therefore, very few studies have investigated the rheological properties of silicate perovskite directly. Among them are micro-indentation hardness measurements under ambient conditions [11], shear stress estimations up to 60 GPa using an approximate relation between pressure gradient and uniaxial stress component in the diamond anvil cell [12], shear stress measurements up to 20 GPa and 1073 K in large volume press [13], electron microscopy analysis of samples quenched from multianvil experiments [14], and lattice preferred orientation (LPO) analysis of samples quenched from high pressure diamond anvil cell experiments [15]. However, the understanding of the rheology of silicate perovskite is still in its infancy. Most studies on lower mantle deformation are still based on analogies with $CaTiO_3$ perovskite ([1,7,9] for instance) in spite of the considerable uncertainties indicated above.

In recent years, a new diamond anvil cell X-ray diffraction technique has been developed to study the strength and elasticity of materials under high pressure [16–24]. This technique later emerged as a powerful tool to obtain direct observations of the deformation mechanisms and the development of LPO of deep Earth materials in situ at relevant pressure, as demonstrated with pilot experiments on ε-Fe and MgO [25,26]. We applied this method to study the development of textures in $(Mg,Fe)SiO_3$ perovskite with pressure under uniaxial stress and deduce information about its strength and deformation mechanisms at room temperature.

2. Experiment

In this study, we perform a deformation experiment with a diamond anvil cell, analyzing the stress state and polycrystalline texture using X-ray diffraction in a direction orthogonal to the compression axis (Fig. 1). In order to obtain reliable statistics in the analysis, we used an angular-dispersive diffraction technique [26]. The background from the confining beryllium gasket was reduced by drilling an opening along the incoming X-ray path which was filled with a mixture of amorphous boron and epoxy to maintain the gasket's mechanical stability. The perovskite sample with a Fe/(Fe+Mg) ratio of 0.01 was synthesized from $(Mg,Fe)SiO_3$ orthopyroxene on the multianvil apparatus of the Center for High Pressure Research. The grain size was reduced to the order of a couple of μm by crushing the chips extracted from the multianvil runs between tungsten carbide cubes. The sample was then loaded and repeatedly pressed until fully compacted in a 100 μm hole along with ruby chips and a layer of polycrystalline platinum. To ensure homogeneous stress conditions in all sections of the sample, diamond anvils with 500 μm tip diameters were used. The measurements were performed on the ID-30 beamline of the European Synchrotron Radiation Facility in Grenoble, using a monochromatic beam of wavelength 0.3738 Å and the in-house fast-scan detector. Each pattern took 1–5 min to record. Details on the experimental technique and data reduction are given elsewhere [26].

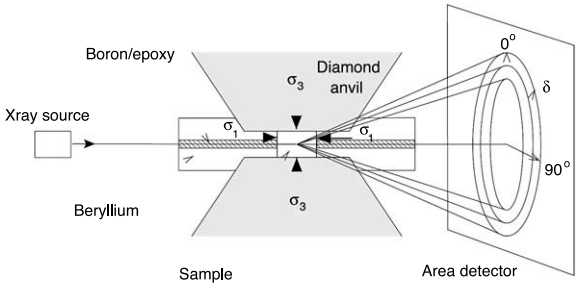

Fig. 1. Schematic of the experiment. The perovskite aggregate is confined under non-hydrostatic stress conditions between two diamond anvils. A monochromatic X-ray beam is sent through the gasket with a direction orthogonal to the diamond axis and the data collected on an area detector orthogonal to the incoming beam. The positions and intensities of the diffraction lines are analyzed as a function of the azimuthal angle δ.

Pressures were estimated using the ruby scale, the equation of state of platinum [27] and that of perovskite itself [28]. We collected data upon compression between 0 and 32 GPa, and decompression between 32 and 1 GPa. However, above 20 GPa in compression the large peak widths and

low diffraction intensities of perovskite made the analysis impossible. This can be attributed to an increase in stress inhomogeneities between grains with compression. These problems disappeared upon decompression as we relaxed the sample. Therefore the results presented here will range between 0 and 19 GPa upon compression and 32 and 1 GPa upon decompression. The distance between the diamond anvils, estimated by recording changes in X-ray absorption while moving the diamond cell in a direction perpendicular to the incoming beam, shows a continuous decrease from 32 to 7 μm during compression to 32 GPa and a continuous increase from 7 to 10 μm during decompression (Fig. 2). Upon compression, this is a good estimation of the sample thickness. Because the deformation is continuous over the whole pressure range, we estimate that it cannot be attributed to compaction and that our sample was submitted to 65% plastic deformation. In order to reduce the background from the sample environment, a diffraction image was collected after removing the sample from the incident beam at each pressure and dividing the diffraction pattern from the sample by this image. The processed diffraction images were then divided into small arcs of 10° intervals to determine the influence of the azimuthal angle δ on the pattern. Figs. 3 and 4 show a representative diffraction pattern at 19 GPa and the spectra we extracted for δ between 0 and 360° with 10° intervals, respectively. In Fig. 4, the variations of the peak posi-

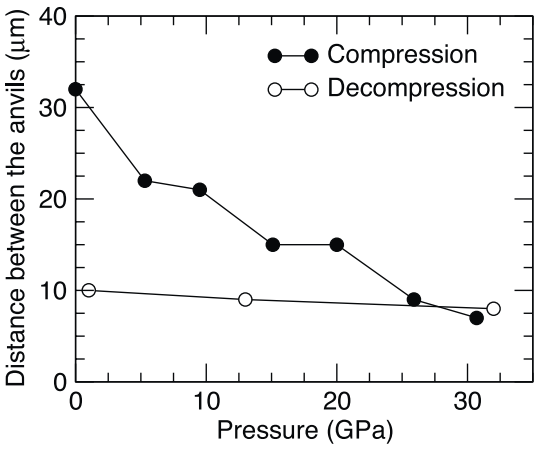

Fig. 2. Distance between the diamond anvils as a function of pressure. Upon compression, this is a good estimation of the sample thickness. From this figure, we estimate that the plastic deformation imposed on the sample is of the order of 65%.

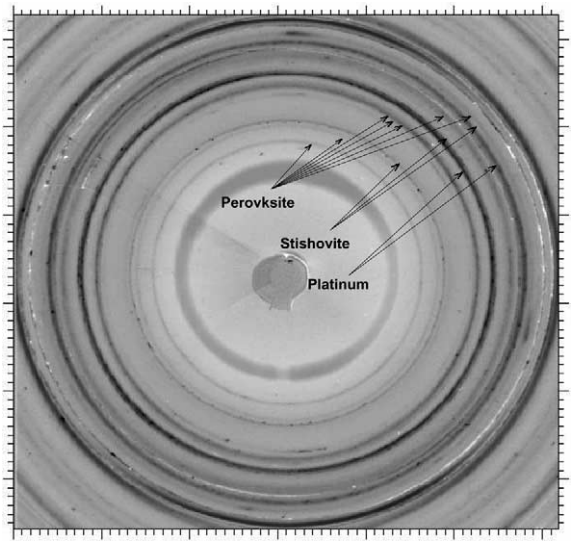

Fig. 3. Representative diffraction pattern at 19 GPa after removing the signal from the background. Selected diffraction lines for perovskite, stishovite (left over from synthesis) and platinum (pressure calibrant) are indicated.

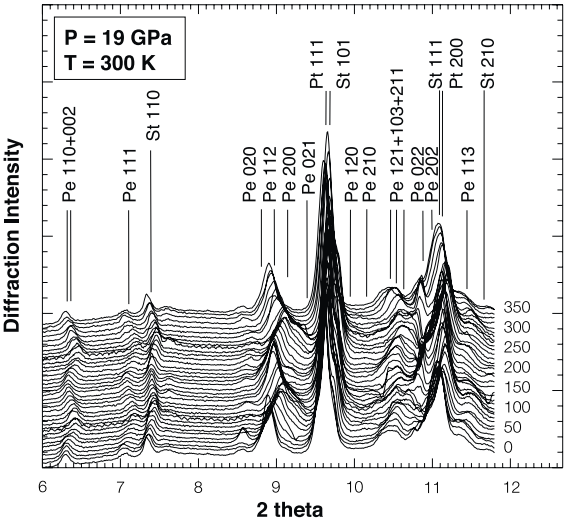

Fig. 4. Spectra extracted from the diffraction pattern at 19 GPa (Fig. 3) for δ between 0 and 360° with 10° intervals. Diffraction lines for perovskite (Pe), platinum (Pt) and stishovite (St) are labeled in the figure.

tion with δ are related to elastic deformation due to non-hydrostatic stress while the variation of the diffraction intensities can be attributed to LPO. For the following analysis, data for the (002) and (110), (111), (020), (112), (200), and (113) peaks of silicate perovskite were fitted using pseudo-Voigt peak profiles.

3. Results

Samples in these diamond anvil cell experiments are subjected to a non-hydrostatic stress, where the principal stress in the loading direction, σ_3, is greater than the radial stress, σ_1, imposed by the gasket. The angle χ between the diffracting plane normal and the maximum stress axis can be calculated from the azimuth angle on the detector, δ, with the relation:

$$\cos\chi = \cos\theta\cos\delta \quad (1)$$

where θ is the diffraction angle. Assuming a Reuss–Voigt–Hill micromechanical model and neglecting the effect of preferred orientations, the measured d-spacings vary with χ as:

$$d_m(hkl) = d_P(hkl)[1 + (1-3\cos^2\chi)Q(hkl)] \quad (2)$$

where $d_m(hkl)$ is the measured d-spacing, $d_P(hkl)$ the d-spacing under the equivalent hydrostatic pressure P, and $Q(hkl)$ is a function of the Miller indices, lattice parameters, and elastic moduli [18]. The variations of the d-spacings of the (112) planes of perovskite with χ upon compression and decompression are shown in Fig. 5 along with results from least-squares fits of Eq. 2. The good agreement between the measured and theoretically predicted χ dependence of the d-spacing assesses the quality of the experimental data. The results of these least-squares fits can then be used to estimate the uniaxial stress component supported by the sample with the relation:

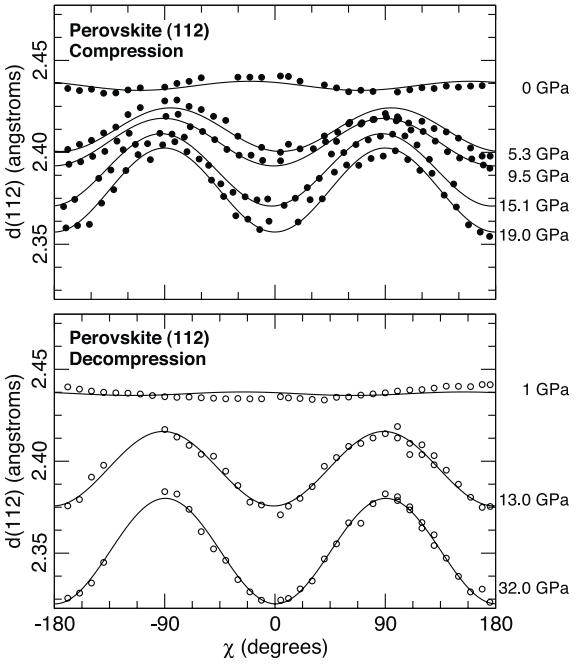

Fig. 5. Variation of the d-spacing of the (112) plane of perovskite as a function of χ upon compression and decompression. Symbols and solid line are experimental data and least-squares fits of a Reuss–Voigt–Hill micromechanical model to the data.

Table 1
Pressure, distance between the anvils, and uniaxial stress component $t = \sigma_3 - \sigma_1$ in perovskite calculated from the measured $\langle Q \rangle$ and the shear modulus G deduced from first-principles calculations [29]

P (GPa)	h (μm)	$\langle Q \rangle$ ($\times 10^3$)	G (GPa)	t (GPa)
0.0 ± 0.1	32	−0.4 ± 0.2	178.6 ± 0.2	−0.4 ± 0.2
5.3 ± 0.3	22	3.1 ± 0.4	186.9 ± 0.5	3.4 ± 0.4
9.5 ± 0.5	21	3.7 ± 0.5	193.4 ± 0.8	4.3 ± 0.6
15.1 ± 0.3	15	5.0 ± 0.6	201.9 ± 0.5	6.0 ± 0.7
19.0 ± 0.5	15	5.3 ± 1.3	207.8 ± 0.7	6.6 ± 1.6
32.0 ± 1.0	8	8.0 ± 1.3	226.8 ± 1.4	10.9 ± 1.9
13.0 ± 0.3	9	4.7 ± 0.9	198.7 ± 0.5	5.6 ± 1.1
1.0 ± 0.5	10	−0.1 ± 0.1	180.2 ± 0.8	−0.1 ± 0.1

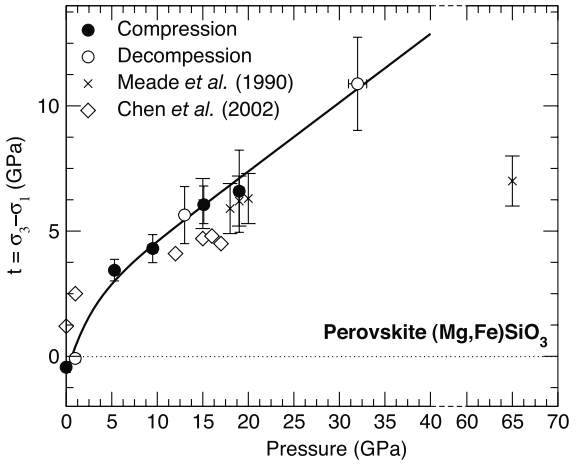

Fig. 6. Uniaxial stress component $t=\sigma_3-\sigma_1$ in perovskite vs. pressure. Closed and open circles are data upon compression and decompression, respectively, crosses are the results of [12] measured using the pressure gradient method, open diamonds are results of multianvil experiments [13], and solid line is a fit to the data of this experiment.

$$t=\sigma_3-\sigma_1\approx 6G\langle Q(hkl)\rangle \quad (3)$$

where G is the shear modulus of the aggregate [18]. Since no experimental measurement of the shear modulus of perovskite in the present pressure range was available, results from first-principles calculations were used [29]. The results we obtained are presented in Table 1 and Fig. 6. Above 2 GPa the uniaxial stress in our sample increases linearly with pressure up to 10.9(±1.9) GPa at 32 GPa. The values of uniaxial stress in the sample deduced upon compression and decompression cannot be distinguished.

In order to study the development of LPO with compression, we use the relative intensity variations of diffraction peaks to calculate the orientation distribution function (ODF) of the sample, which contains all information about the crystallite orientations and can be used for deformation mechanism analysis. Fig. 7 presents the measured diffraction intensities for the (110)+(002), (020), (112) (200) and (113) diffraction lines of perovskite at the end of the decompression along with those recalculated from the ODF. There is considerable dispersion in the experimental data and no clear systematic variation of intensities with χ can be observed, except for the weak reflection (200). The texture in the sample is axially symmetric around the compression axis, consistent with deformation performed in axial compression. It is therefore most efficiently displayed in the form of

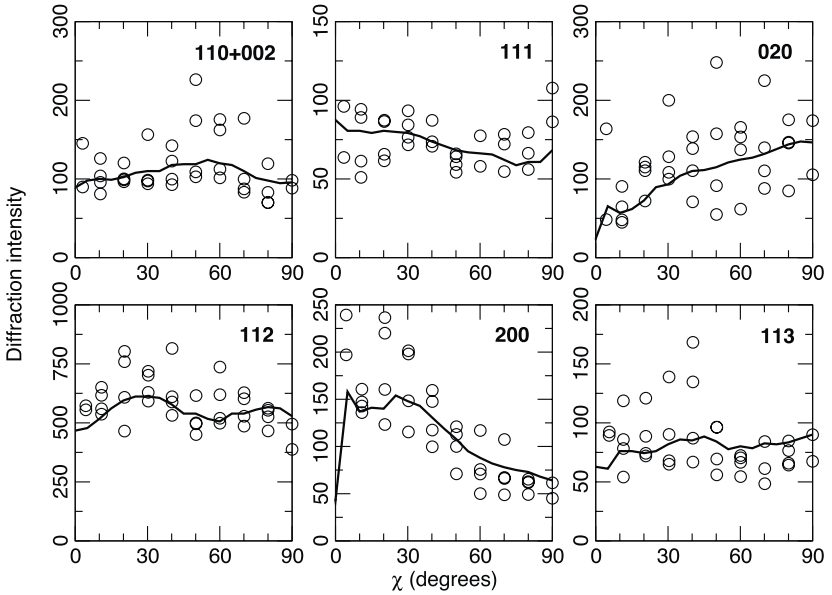

Fig. 7. Diffraction intensities vs. χ for perovskite at the end of the decompression. Open circles are experimental data and solid lines are recalculated from the ODF.

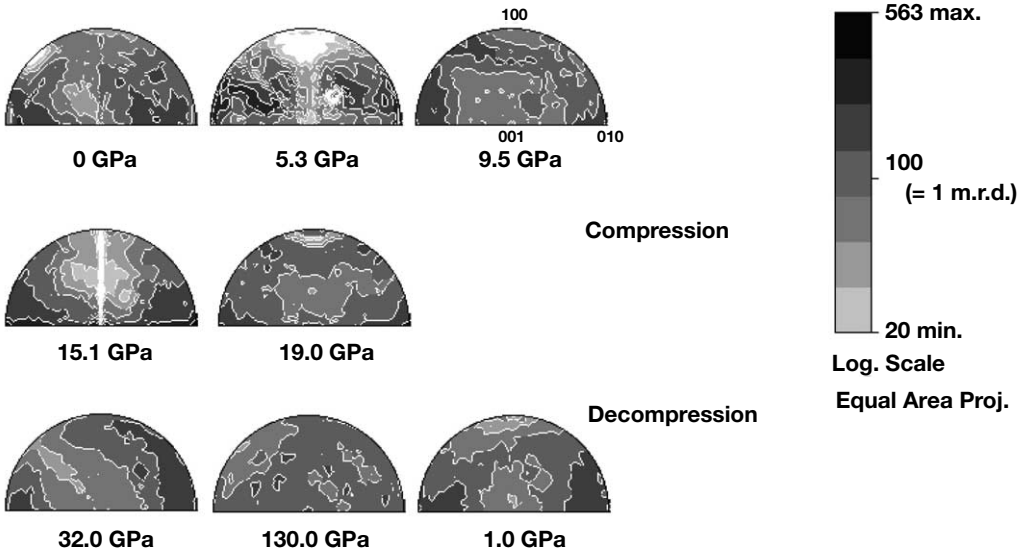

Fig. 8. Experimental inverse pole figures for perovskite upon compression and decompression.

inverse pole figures (Fig. 8), which show the orientation distribution of the experimental compression axis relative to the crystallographic coordinate system of the orthorhombic perovskite structure. The inverse pole figures show no significant changes with compression or decompression, which implies that the sample did not develop any significant LPO in this experiment. This is also apparent in Fig. 4, which shows very little intensity variation with angle, for instance for reflections (110)+(002), (111) and (113).

4. Discussion

According to the von Mises yielding criterion, the measured uniaxial stress (Fig. 6) provides a lower bound on the yield strength of perovskite as $t = \sigma_3 - \sigma_1 \leq \sigma_y$, where σ_y is the yield strength. The uniaxial stress varies with sample environment and equality holds only if the sample deforms plastically. It should also be noted that the experiments presented here are different from mechanical tests at a given pressure, temperature, and imposed strain-rate. In these experiments, strain, strain rate and pressure cannot be decoupled and therefore we rely on a more general definition of the yield strength that may include effects of hardening. Above 2 GPa, we find $t = 1.8(3) + 0.28(2)P$ where t and P are in GPa. Therefore:

$$\sigma_y \geq 1.8(3) + 0.28(2)P \quad (4)$$

for perovskite up to 30 GPa, where σ_y and P are in GPa. Comparison with other measurements of uniaxial stress in perovskite is shown in Fig. 6. Between 15 and 25 GPa, our results agree with those of [12] and [13]. However, the saturation observed above 25 GPa in [12] is not seen in our experiments. As mentioned above, the uniaxial stress is only a lower bound on the yield strength and its actual value depends on sample environment. Our results are thus not incompatible with the previous work since t might have saturated in their experiments for a variety of reasons. One should also point out, however, that these authors used a technique based on measuring the pressure gradient across the diamond anvil and estimating t by $t \approx h(\mathrm{d}P/\mathrm{d}r)$ where h is the sample thickness and r the radial distance from the center of the diamond. The sample thickness is poorly estimated at high pressure; moreover, the above relation holds only if the sample continues to flow plastically on each loading. Arrest of plastic flow often occurs in the vicinity of the maximum pressures of these experiments, as does

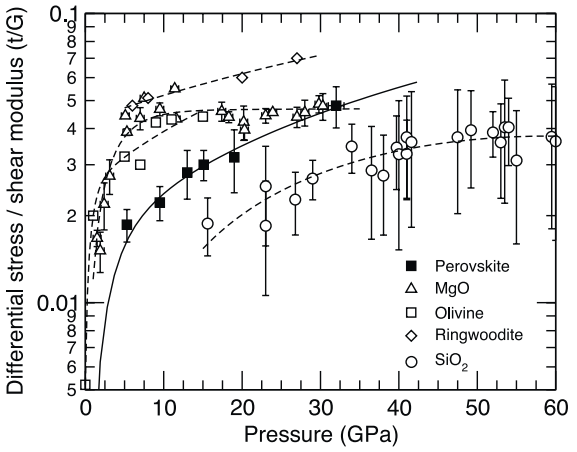

Fig. 9. Ratio of uniaxial stress component to shear modulus t/G as a function of pressure. Solid squares are measurements on perovskite from this study, open triangles, squares, diamonds, and circles are results for MgO [26], olivine [32], ringwoodite [22], and SiO_2 [24], respectively.

the increase of uniaxial stress below the diamond tips [30]. We conclude that the saturation previously observed is not intrinsic to perovskite and that its yield strength can be well over 10 GPa at a pressure of 30 GPa at room temperature, making it one of the hardest silicates of the Earth's interior. This conclusion is consistent with that of [13] based on measurements up to 20 GPa and 1073 K, where perovskite was shown to display very little relaxation and became much stronger than other silicates, such as ringwoodite, upon heating.

The dimensionless parameter τ/G, where τ is the shear strength and G the shear modulus, is a useful quantity for comparing strength between different materials [31]. Moreover, the quantity t/G is measured directly in the radial diffraction experiments (e.g. Eq. 3) and no bulk parameter needs to be assumed. Fig. 9 shows the results we obtain for perovskite along with measurements on olivine [32], ringwoodite [22], MgO [26], and SiO_2 [24]. The t/G ratio for perovskite at ambient temperature lies between those of SiO_2 and the other silicates. Notably, the trend for $(Mg,Fe)SiO_3$ is quite similar to that observed for SiO_2 (stishovite and $CaCl_2$-type), which also has Si in octahedral coordination.

However, the representation of uniaxial stress as a function of pressure has been problematic: results from different experiments can be inconsistent and the evolution of t or t/G with pressure tends to be highly non-linear. Fig. 10 presents the evolution of the normalized uniaxial stress t/G with macroscopic strain $\gamma=(h_0-h)/h_0$ where h is the distance between the anvils (e.g. Table 1). In this representation the evolution of uniaxial stress can be easily decomposed into two domains where t evolves linearly with γ (i.e. increasing strain and decreasing strain). In our experiments, pressure, strain, and uniaxial stress cannot be decoupled. Therefore a comparison with results from mechanical tests at constant pressure, temperature and strain rate is not trivial. However, because strain is strongly related to plastic deformation, we feel that this representation should provide valuable information when data from other experiments become available.

The absence of LPO in perovskite in our experiments is consistent with previous observations on $(Mg,Fe)SiO_3$ perovskite [15]. In those experiments, perovskite had been deformed under uniaxial compression in the diamond anvil cell and quenched to ambient conditions. No texture could be observed. In our experiments, we followed the development of texture under uniaxial compression in situ up to 30 GPa, with 10 GPa uniaxial stress at the highest pressures, after 65% plastic

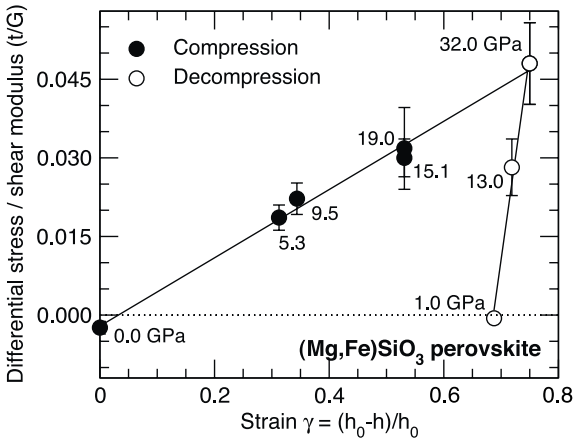

Fig. 10. Normalized uniaxial stress component t/G in perovskite vs. strain. Closed and open circles are data upon compression and decompression, respectively. Solid lines are linear fits to the data from 0 to 32 GPa and from 32 to 0 GPa.

deformation, and a homologous temperature $T/T_m \approx 0.1$, and found no clear sign of LPO. Although further experiments are required to identify the specific deformation mechanism, the absence of significant LPO indicates that plastic deformation by dislocation is not dominant. This is in agreement with deduction from high temperature relaxation at high pressure where the evolution of stress and strain in perovskite was shown to be incompatible with both dislocation glide and power-law creep [13]. This has also been documented for fine-grained $CaTiO_3$, from which it was inferred that silicate perovskite undergoes superplastic deformation [7]. Deformation mechanisms depend strongly on stress, temperature and grain size. Thus, the influence of all these factors needs to be further investigated in order to infer the behavior of silicate perovskite in the lower mantle. To this end, the in situ experiments described here should be extended to higher temperature and grain sizes varied.

The major cause for seismic anisotropy in the deep Earth is elastic anisotropy combined with LPO. Therefore, a perovskite aggregate deformed in conditions similar to those of this study would not generate any seismic anisotropy. While the effect of higher temperature, controlled strain rate and grain size should be investigated to fully understand the rheology of silicate perovskite in the deep mantle, our in situ experiments have demonstrated the feasibility of direct investigations on the strength and deformation mechanisms of silicate perovskite under high pressure. The lack of significant LPO in perovskite is in contrast with similar experiments on another lower mantle mineral, magnesiowuestite, where strong LPO was observed at low temperature and high pressure [26].

Seismological observations about the anisotropy in the deep mantle have only recently been well documented. There have been numerous reports of anisotropy in its lowermost boundary layer, D″ (e.g. [33,34]), and near the 660 km discontinuity [35,36] the few studies that concentrated on the mid-to-lower mantle region found little evidence for anisotropy [15,35]. These studies, however, were limited in global coverage and recent numerical calculations assuming composite mantle rheology have shown that the deformation of subducting slabs in the lower mantle occurs mostly by dislocation creep and could therefore exhibit significant anisotropy [1,37]. Reliably detecting anisotropy in these regions requires careful seismological experiments. Moreover, interpreting data from geological settings which exhibit 3D variations in heterogeneity and anisotropy is difficult as the nature of wave propagation in such complex settings is not well understood [34]. Recent experiments have documented the development of significant LPO in magnesiowuestite, both under low pressure and high temperature [38,39] and high pressure and low temperature [26]. In contrast, our experiments have shown that it is extremely difficult to generate significant LPO in silicate perovskite. Although the critical parameters of the effect such as temperature and grain size should be investigated for a direct comparison with the lower mantle, this implies that perovskite is less likely to be the source of seismic anisotropy than these other silicates.

Acknowledgements

The authors are grateful to Yingwei Fei for providing the sample and Mohamed Mezouar for assistance during the experiment. We also thank P. Cordier, D. Price, and the anonymous reviewers whose comments significantly improved the manuscript. *[SK]*

References

[1] A.K. McNamara, P.E. van Keken, S. Karato, Development of anisotropic structure in the Earth's lower mantle by solid state convection, Nature 416 (2002) 310–314.
[2] J.P. Poirier, J. Peyronneau, J.Y. Gesland, G. Berbec, Viscosity and conductivity of the lower mantle: an experimental study on a $MgSiO_3$ perovskite analogue, $KZnF_3$, Phys. Earth Planet. Inter. 32 (1983) 273–287.
[3] S. Beauchesne, J.P. Poirier, Creep of barium titanate perovskite: a contribution to a systematic approach to the viscosity of the lower mantle, Phys. Earth Planet. Inter. 55 (1989) 187–199.
[4] S. Beauchesne, J.P. Poirier, In search of a systematics for the viscosity of perovskites: creep of potassium tantalate and niobate, Phys. Earth Planet. Inter. 61 (1990) 182–198.

[5] S. Karato, P. Li, Diffusion creep in perovskite: implications for the rheology of the lower mantle, Science 255 (1992) 1238–1240.
[6] Z. Wang, S. Karato, F. Fujino, High temperature creep of single crystal strontium titanate ($SrTiO_3$): a contribution to creep systematics in perovskites, Phys. Earth Planet. Inter. 79 (1993) 299–312.
[7] S. Karato, S. Zhang, H.R. Wenk, Superplasticity in Earth's lower mantle: evidence from seismic anisotropy and rock physics, Science 270 (1995) 458–461.
[8] P. Besson, J.P. Poirier, G.D. Price, Dislocations in $CaTiO_3$ perovskite deformed at high temperature: a transmission electron microscopy study, Phys. Chem. Min. 23 (1996) 337–344.
[9] P. Li, S. Karato, Z. Wang, High-temperature creep in fine-grained polycrystalline $CaTiO_3$, an analogue material of (Mg, Fe)SiO_3 perovskite, Phys. Earth Planet. Inter. 95 (1996) 19–36.
[10] Z.C. Wang, C. Dupas-Bruzek, S. Karato, High temperature creep of an orthorhombic perovskite - $YAlO_3$, Phys. Earth Planet. Inter. 110 (1999) 51–69.
[11] S. Karato, F. Fujino, E. Ito, Plasticity of $MgSiO_3$ perovskite: the results of microhardness tests on single crystals, Geophys. Res. Lett. 17 (1990) 13–16.
[12] C. Meade, R. Jeanloz, The strength of mantle silicates at high pressure and room temperature: implications for the viscosity of the mantle, Nature 348 (1990) 533–535.
[13] J. Chen, D.J. Weidner, M.T. Vaughan, The strength of $Mg_{0.9}Fe_{0.1}SiO_3$ perovskite at high pressure and temperature, Nature 419 (2002) 824–826.
[14] Y. Wang, F. Guyot, R.C. Liebermann, Electron microscopy of (Mg,Fe)SiO_3 perovskite: evidence for structural phase transition and implications for the lower mantle, J. Geophys. Res. 97 (1992) 12327–12347.
[15] C. Meade, P.G. Silver, S. Kanshima, Laboratory and seismological observations of lower mantle isotropy, Geophys. Res. Lett. 22 (1995) 1293–1296.
[16] R.J. Hemley, H.K. Mao, G. Shen, J. Badro, P. Gillet, M. Hanfland, D. Häusermann, X-ray imaging of stress and strain of diamond, iron, and tungsten at megabar pressures, Science 276 (1997) 1242–1245.
[17] A.K. Singh, H.K. Mao, J. Shu, R.J. Hemley, Estimation of single crystal elastic moduli from polycrystalline X-ray diffraction at high pressure: Applications to FeO and iron, Phys. Rev. Lett. 80 (1998) 2157–2160.
[18] A.K. Singh, C. Balasingh, H.K. Mao, R.J. Hemley, J. Shu, Analysis of lattice strains measured under non-hydrostatic pressure, J. Appl. Phys. 83 (1998) 7567–7575.
[19] H.K. Mao, J. Shu, G. Shen, R.J. Hemley, B. Li, A.K. Singh, Elasticity and rheology of iron above 220 GPa and the nature of the Earth's inner core, Nature 396 (1998) 741–743; correction, Nature 399 (1999) 280.
[20] T.S. Duffy, G. Shen, J. Shu, H.K. Mao, R.J. Hemley, A.K. Singh, Elasticity, shear strength and equation of state of molybdenum and gold from X-ray diffraction under nonhydrostatic compression to 24 GPa, J. Appl. Phys. 86 (1999) 1–8.
[21] T.S. Duffy, G. Shen, D.L. Heinz, J. Shu, Y. Ma, H.K. Mao, R.J. Hemley, A.K. Singh, Lattice strains in gold and rhenium under non-hydrostatic compression to 37 GPa, Phys. Rev. B 60 (1999) 1–10.
[22] A. Kavner, T.S. Duffy, Strength and elasticity of ringwoodite at upper mantle pressures, Geophys. Res. Lett. 28 (2001) 2691–2694.
[23] S. Merkel, A.P. Jephcoat, J. Shu, H.K. Mao, P. Gillet, R.J. Hemley, Equation of state, elasticity and shear strength of pyrite under high pressure, Phys. Chem. Min. 29 (2002) 1–9.
[24] S. Shieh, T.S. Duffy, B. Li, Strength and elasticity of SiO_2 across the stishovite-$CaCl_2$-type structural phase boundary, Phys. Rev. Lett. 89 (2002) 255507.
[25] H.R. Wenk, S. Matthies, R.J. Hemley, H.K. Mao, J. Shu, The plastic deformation of iron at pressures of the Earth's inner core, Nature 405 (2000) 1044–1047.
[26] S. Merkel, H.R. Wenk, J. Shu, G. Shen, P. Gillet, H.K. Mao, R.J. Hemley, Deformation of polycrystalline MgO at pressures of the lower mantle, J. Geophys. Res. 107 (2002) 2271.
[27] N.C. Holmes, J.A. Moriarty, G.R. Gathers, W.J. Nellis, The equation of state of platinum to 660 GPa (6.6 Mbar), J. Appl. Phys. 66 (1989) 2962–2967.
[28] G. Fiquet, D. Andrault, A. Dewaele, T. Charpin, M. Kunz, D. Häusemann, P-v-t equation of state of $MgSiO_3$ perovskite, Phys. Earth Planet. Inter. 105 (1998) 21–31.
[29] R.M. Wentzcovitch, B.B. Karki, S. Karato, C.R.S.D. Silvera, High pressure elastic anisotropy of $MgSiO_3$ and geophysical implications, Earth Planet. Sci. Lett. 164 (1998) 371–378.
[30] S. Merkel, R.J. Hemley, H.K. Mao, D.M. Teter, Finite element modeling and ab-initio calculations of megabar stresses in the diamond anvil cell, in: M. Manghnani, W.J. Nellis, M.F. Nicol (Eds.), Science and Technology of High Pressure Research, University Press (India) Limited, 2000, pp. 68–73.
[31] S. Karato, Plasticity-crystal structure systematics in dense oxides and its implications for the creep strength of the Earth's deep interior: a preliminary result, Phys. Earth Planet. Inter. 55 (1989) 234–240.
[32] T. Uchida, N. Funamori, T. Ohtani, T. Yagi, Differential stress of MgO and Mg_2SiO_4 under uniaxial stress field: Variation with pressure, temperature, and phase transition, in: W.A. Trzeciatowski (Ed.), High Pressure Science and Technology, World Scientific Publishing, Singapore, 1996, pp. 183–185.
[33] T. Lay, Q. Williams, E.J. Garnero, The core-mantle boundary layer and deep Earth dynamics, Nature 392 (1998) 461–468.
[34] J.M. Kendall, Seismic anisotropy in the boundary layers of the mantle, in: S. Karato, A.M. Forte, R.C. Liebermann, G. Master, L. Stixrude (Eds.), Earth's Deep Interior. Mineral Physics and Tomography. From the Atomic to the Global Scale, Am. Geophys. Union, Washington, DC, 2000, pp. 133–159.
[35] J.P. Montagner, Where can seismic anisotropy be detected

in the Earth's mantle? in the boundary layers..., Pure Appl. Geophys. 151 (1998) 223–256.
[36] J. Wookey, J.M. Kendall, G. Barruol, Mid-mantle deformation inferred from seismic anisotropy, Nature 415 (2002) 777–780.
[37] A.K. McNamara, S.I. Karato, P.E. van Keken, Localization of dislocation creep in the lower mantle: implications for the origin of seismic anisotropy, Earth Planet. Sci. Lett. 191 (2001) 85–99.
[38] I. Stretton, F. Heidelbach, S. Mackwell, F. Langenhorst, Dislocation creep of magnesiowüstite ($Mg_{.8}Fe_{0.2}O$), Earth Planet. Sci. Lett. 194 (2001) 229–240.
[39] D. Yamazaki, S. Karato, Fabric development in (Mg, Fe)O during large strain, shear deformation: implications for seismic anisotropy in Earth's lower mantle, Phys. Earth Planet. Inter. 131 (2002) 251–267.